# An approach to multi-body interactions in a continuum-atomistic context: Application to analysis of tension instability in carbon nanotubes

K.Y. Volokh *, K.T. Ramesh

*Department of Mechanical Engineering, Johns Hopkins University, 3400 North Charles Street, Baltimore, MD 21218, USA*

## Abstract

The tensile strength of single-walled carbon nanotubes (CNT) is examined using a continuum-atomistic (CA) approach. The strength is identified with the onset of the CNT instability in tension. The focus of this study is on the effects of multi-body atomic interactions. Multiscale simulations of nanostructures usually make use of two- and/or three-body inter-atomic potentials. The three-body potentials describe the changes of angles between the adjacent bonds – bond bending. We propose an alternative and simple way to approximately account for the multi-body interactions. We preserve the pair structure of the potentials and consider the multi-body interaction by splitting the changing bond length into two terms. The first term corresponds to the self-similar deformation of the lattice, which does not lead to bond bending. The second term corresponds to the distortional deformation of the lattice, which does lead to bond bending. Such a split of the bond length is accomplished by means of the spherical–deviatoric decomposition of the Green strain tensor. After the split, the continuum-atomistic potential can be written as a function of two bond lengths corresponding to the bond stretching and bending independently. We apply an example exponential continuum-atomistic potential with the split bond length to the study of tension instability of the armchair and zigzag CNTs. The results of the study are compared with those obtained by Zhang et al. (2004. J. Mech. Phys. Solids 52, 977–998) who studied tension instability of carbon nanotubes by using the Tersoff–Brenner three-body potential, and with recent experimental results on the tensile failure of single walled carbon nanotubes.
© 2006 Elsevier Ltd. All rights reserved.

*Keywords:* Continuum-atomistic analysis; Interatomic potential; Carbon nanotube

## 1. Introduction

Materials science, biomedical engineering and medicine are just a few fields, which benefit from the development of nanotechnology. This technology allows for design and production of atomic assemblies and

_____

* Corresponding author. On leave of absence from the Technion–Israel Institute of Technology.
  *E-mail addresses:* kvolokh@jhu.edu, cvolokh@tx.technion.ac.il (K.Y. Volokh).

devices at the nanoscale including carbon nanotubes (Goddard et al., 2003; Dresselhaus et al., 1996; Harris, 1999; Meyyappan, 2005; Qian et al., 2002; Reich et al., 2004) and nanocomposites (Alexandre and Dubois, 2000; Beecrot and Ober, 1997; Odegard et al., 2002). Nanotube assemblies, in particular, can be regarded as small structures undergoing deformation, vibrations, buckling and fracture. From this perspective, analysis of mechanical behavior of nanostructures is of interest.

It is natural to apply the methods of quantum mechanics (QM) and/or molecular dynamics (MD) at the nanoscale. However, such methods quickly become computationally intensive as the number of atoms increase. This has led to the development of multiple-scale approaches where atomistic and continuum models are coupled. There are a number of ways to make this coupling. For example, Abraham et al. (1998) and Broughton et al. (1999) developed the MAAD approach where macroscopic, atomistic and ab initio (tight-binding) dynamics are linked together to simulate the processes of brittle fracture around a crack-tip in silicon. Another approach, called the quasi-continuum (QC) method, was developed in a series of papers by Tadmor et al. (1996), Shenoy et al. (1998), Miller et al. (1998), and Ortiz et al. (2001). In the QC method, the interatomic potentials are enhanced with the continuum deformation gradients through the Cauchy–Born rule. In a third approach, Liu and co-workers (2004) developed a concurrent-coupling method where a hierarchical structure of the displacement field is introduced and used in different types of numerical simulations.

Among the problems where coupled continuum-atomistic analysis is desirable, the mechanical behavior of carbon nanotubes (CNT) stands out. The discovery of CNTs (Iijima, 1991; Ebbesen and Ajayan, 1992) and the development of effective manufacturing techniques (Thess et al., 1996) led to an explosion of interest and research in the field. CNT radii are usually of the order of one nanometer and the CNT length can vary from a few nanometers to tens of nanometers. The experimentally measured stiffness (Young's modulus) is remarkable, of the order of TeraPascals (Treacy et al., 1996; Wong et al., 1997; Krishnan et al., 1998; Lourie and Wagner, 1998a; Muster et al., 1998; Pan et al., 1999; Salvetat et al., 1999; Tombler et al., 2000; Yu et al., 2000). Further, the critical fracture strain computed by using different techniques ranges from 10% to 50%. For example, Yakobson et al. (1997) obtained a fracture strain ranging from 30% to 50% using MD simulations based on the Brenner (1990) interatomic potential. Zhang et al. (2004) used a continuum-atomistic analysis considering the onset of fracture as the tension instability of the CNT and obtained a critical strain ranging from 30% to 40%. Belytschko et al. (2002) found a critical strain between 10% and 16% by using MD simulations with the modified Morse interatomic potential. Experimental results on the tensile failure of single-wall carbon nanotubes (SWCNTs) are relatively rare. Lourie and Wagner (1998b) observed the fracture of bundles of single-wall CNTs in a TEM (the CNTs were reinforcements in an epoxy matrix) but did not obtain quantitative information on either critical or failure strains. Marques et al. (2004) present a more detailed discussion of the high-resolution TEM experiments of Troiani et al. (2003) in which a single SWCNT was failed in tension while under observation; the resulting failure strain was approximately 50%. An excellent summary of recent experimental work is presented in a review article by Yu (2004).

The focus of the present study is twofold. First, we aim to develop a novel approach to account for the multi-body atomic interactions in a continuum-atomistic calculation. Next, we aim to use this approach to study the critical fracture strain under the tension of CNTs defining the onset of fracture as the bifurcation of the CNT equilibrium in tension (Zhang et al., 2004). Existing approaches usually make use of two- and/or three-body interatomic potentials. The three-body potentials describe the changes of angles between the adjacent bonds – the bond bending. We propose an alternative and simple way to account for the multi-body interactions. The idea is to preserve the pair structure of the potentials but to consider the multi-body interaction by splitting the changing bond length into two terms. The first term corresponds to the self-similar deformation of the lattice, which does not lead to bond bending. The second term corresponds to the distortional deformation of the lattice, which does lead to bond bending. Such a split of the bond length is accomplished by means of the spherical–deviatoric decomposition of the Green strain tensor. After the split, the continuum-atomistic potential can be written as a function of two bond lengths corresponding to the bond stretching and bending independently. This double split (continuum and atomistic) presents further elaboration of the ideas put forward in Volokh (2004) and Volokh and Gao (2005). We apply an example exponential continuum-atomistic potential with the split bond length to the study of tension instability of armchair and zigzag CNTs.

## 2. Continuum-atomistic coupling

In this section, we consider the interatomic potentials (Section 2.1), the continuum link through the Cauchy–Born rule (Section 2.2), and the split continuum-atomistic potential (Section 2.3). The results of this section are used in the study of the CNT instability in Section 3.

### 2.1. Interatomic potentials

Consider a solid body $\Omega$ comprising atoms located at $\mathbf{r}_i$ in the 3D space. Generally, the total potential energy of the body is a function of the particle positions: $Y(\mathbf{r}_1, \mathbf{r}_2, \ldots, \mathbf{r}_n)$, where $n$ is the number of particles. Specifically for carbon, Tersoff (1988) and Brenner (1990) suggest

$$Y^C = \frac{1}{2} \sum_{i,j} U(r_{ij}), \tag{2.1}$$

where

$$U(r_{ij}) = \frac{D}{S-1} f_c(r_{ij}) \left\{ \exp\left[-\sqrt{2S}\beta(r_{ij} - R_{ij})\right] - SB_{(ij)} \exp\left[-\sqrt{2/S}\beta(r_{ij} - R_{ij})\right] \right\}, \tag{2.2}$$

$$r_{ij} = \sqrt{(\mathbf{r}_i - \mathbf{r}_j) \cdot (\mathbf{r}_i - \mathbf{r}_j)}, \tag{2.3}$$

$$R_{ij} = \sqrt{(\mathbf{R}_i - \mathbf{R}_j) \cdot (\mathbf{R}_i - \mathbf{R}_j)}. \tag{2.4}$$

Here $\mathbf{R}_i$ is the initial equilibrium position of the $i$th atom; $D = 6.0$ eV; $S = 1.22$; $\beta = 21$ nm$^{-1}$; and $R_{ij} = 0.145$ nm is the equilibrium bond length for atoms $i$ and $j$ under the condition of multi-atomic coupling (Zhang et al., 2004).

The cutoff function $f_c(r_{ij})$ used in (2.2) is

$$f_c = \begin{cases} 1, & r_{ij} < a_1, \\ \dfrac{1}{2} + \dfrac{1}{2} \cos \dfrac{\pi(r_{ij} - a_1)}{a_2 - a_1}, & a_1 < r_{ij} < a_2, \\ 0, & r_{ij} > a_2 \end{cases} \tag{2.5}$$

with $a_1 = 0.17$ nm and $a_2 = 0.20$ nm to include the only the first-neighbor shell for carbon.

The function representing the three-body coupling $B_{(ij)} = (B_{ij} + B_{ji})/2$ is

$$B_{ij} = \left\{ 1 + \sum_{k(\neq i,j)} a_0 \left( 1 + \frac{c_0^2}{d_0^2} - \frac{c_0^2}{d_0^2 + (1 + \cos\varphi_{ijk})^2} \right) f_c(r_{ij}) \right\}^{-\delta}, \tag{2.6}$$

$$\cos\varphi_{ijk} = \mathbf{r}_{ij} \cdot \mathbf{r}_{ik} / (r_{ij} r_{ik}), \tag{2.7}$$

where $a_0 = 0.00020813$, $c_0 = 330$, $d_0 = 3.5$, $\delta = 0.5$.

This three-body carbon potential was applied to CNT continuum-atomistic analysis by Zhang et al. (2004). Other potentials accounting for two- and three-body interactions can also be found in the literature with various cutoff functions. However, the potential presented by Eqs. (2.1)–(2.7) will be utilized in this paper for comparison purposes and for the assessment of the results of our analysis.

### 2.2. Cauchy–Born rule

According to the Cauchy–Born rule, originally applied to crystal elasticity (Born and Huang, 1954; Weiner, 1983), the current $\mathbf{r}_{ij} = \mathbf{r}_i - \mathbf{r}_j$ and initial (equilibrium) $\mathbf{R}_{ij} = \mathbf{R}_i - \mathbf{R}_j$ relative positions of the same two atoms can be related as follows:

$$\mathbf{r}_{ij} = \mathbf{F} \mathbf{R}_{ij}, \tag{2.8}$$

with the help of the deformation gradient

$$\mathbf{F} = \nabla\boldsymbol{\chi}(\mathbf{X}), \tag{2.9}$$

where $\boldsymbol{\chi}(\mathbf{X})$ is the current position of the referential point $\mathbf{X}$ and the $i$th and $j$th atoms are found in the vicinity of the point $\mathbf{X}$ – Fig. 1.

Substitution of Eq. (2.8) in Eq. (2.1) allows one to define the potential energy density $W$ in terms of the Green strain tensor $\mathbf{E}$ over representative volume $V_0$:

$$W = \frac{1}{2V_0} \sum_{i,j} U(r_{ij}) = W(\mathbf{E}), \tag{2.10}$$

where

$$r_{ij} = \sqrt{\mathbf{R}_{ij} \cdot (\mathbf{1} + 2\mathbf{E})\mathbf{R}_{ij}}, \tag{2.11}$$

$$\cos \varphi_{ijk} = \mathbf{R}_{ij} \cdot (\mathbf{1} + 2\mathbf{E})\mathbf{R}_{ik} / (r_{ij} r_{ik}), \tag{2.12}$$

$$\mathbf{E} = (\mathbf{F}^{\mathrm{T}}\mathbf{F} - \mathbf{1})/2. \tag{2.13}$$

Here $\mathbf{1}$ is the second-order identity tensor.

The second Piola–Kirchhoff stress tensor and the fourth-order tangent stiffness tensor can then be calculated from the strain energy function:

$$\mathbf{S} = \partial W/\partial \mathbf{E}, \tag{2.14}$$

$$\mathbf{C} = \partial \mathbf{S}/\partial \mathbf{E}. \tag{2.15}$$

**Remark 1.** The basic formulation of the Cauchy–Born rule described above is applicable to the case of a simple lattice. In the case of a multi-lattice, it is necessary to introduce additional vectors of atomic displacements, which represent the atomic relaxation processes after deformation. In the case of the complex lattice comprising two simple sub-lattices, for example, we have to replace Eq. (2.8) with

$$\mathbf{r}_{ij} = \mathbf{F}\mathbf{R}_{ij} + \boldsymbol{\gamma} = \mathbf{F}(\mathbf{R}_{ij} + \boldsymbol{\beta}), \tag{2.16}$$

where vectors $\boldsymbol{\gamma}$ and $\boldsymbol{\beta} = \mathbf{F}^{-1}\boldsymbol{\gamma}$ designate a possible shift between the two sub-lattices. These vectors are introduced in order to account for the relaxation of the atomic positions providing the equilibrium of atoms. The shift vector is determined by minimizing the strain energy density with respect to $\boldsymbol{\beta}$ (Weiner, 1983; Tadmor et al., 1999; Arroyo and Belytschko, 2002):
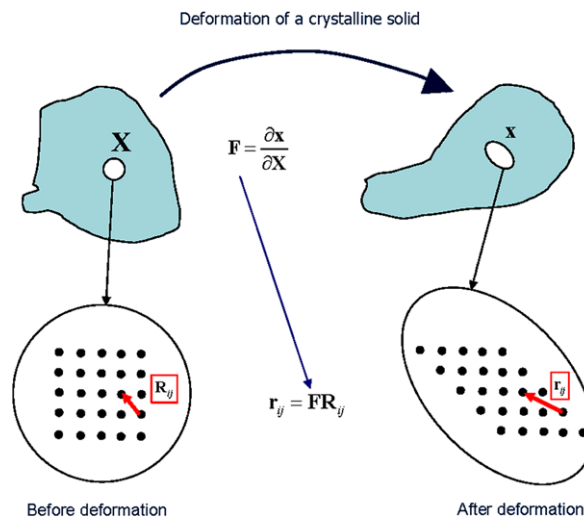


Fig. 1. Cauchy–Born rule – scale linking.

$$\frac{\partial W(\mathbf{E}, \boldsymbol{\beta})}{\partial \boldsymbol{\beta}} = \mathbf{0}. \tag{2.17}$$

Solving this equation it is possible to obtain $\boldsymbol{\beta}$ as a function of $\mathbf{E}$. Now the second Piola–Kirchhoff stress tensor can be calculated from the strain energy function by using the chain rule

$$\mathbf{S} = \frac{\partial W}{\partial \mathbf{E}} + \frac{\partial W}{\partial \boldsymbol{\beta}} \frac{\partial \boldsymbol{\beta}}{\partial \mathbf{E}} = \frac{\partial W}{\partial \mathbf{E}}. \tag{2.18}$$

The tangent stiffness moduli can be derived by further differentiation

$$\mathbf{C} = \frac{\partial \mathbf{S}}{\partial \mathbf{E}} = \frac{\partial^2 W}{\partial \mathbf{E}\, \partial \mathbf{E}} - \frac{\partial^2 W}{\partial \boldsymbol{\beta}\, \partial \mathbf{E}} \left( \frac{\partial^2 W}{\partial \boldsymbol{\beta}\, \partial \boldsymbol{\beta}} \right)^{-1} \frac{\partial^2 W}{\partial \mathbf{E}\, \partial \boldsymbol{\beta}}, \tag{2.19}$$

where the result of differentiation of Eq. (2.17) with respect to $\mathbf{E}$ has been used.

Generally, the shift appears because symmetries break during the deformation. However, in the particular case of the tension instability of the zigzag and armchair nanotubes, which will be considered in the next section, the symmetries are preserved during the simple tension in the pre-bifurcation state and, consequently, there is no need to account for the atomic relaxation. The symmetries break, of course, after the bifurcation of the equilibrium state. The post-bifurcation behavior, however, is beyond the scope of this study. In summary, we will ignore the shift vector between two sub-lattices of the zigzag and armchair CNTs in subsequent considerations.

**Remark 2.** Direct use of Eq. (2.10) in analysis of material behavior can be difficult because of the large number of atoms in a representative volume. In this case, the sum of the bond potentials can be replaced with the integral as follows:

$$W = \langle U \rangle = W(\mathbf{E}), \quad \langle U \rangle = \frac{1}{V_0} \int_{V_0^*} U D_{\mathrm{V}}\, \mathrm{d}V, \tag{2.20}$$

where $V_0$ is the reference representative volume; $D_{\mathrm{V}}$ is the volumetric bond density function; and $V_0^*$ is the integration volume defined by the range of influence of $U$ (Gao and Klein, 1998; Klein and Gao, 1998, 2000).

### 2.3. Split continuum-atomistic potential

The Cauchy–Born approach described in the two previous subsections is a mixture of atomistic and continuum concepts. However, the concept of the continuum deformation appears only at the last stage of the model formulation when Eq. (2.10) is used. Thus, the choice of the interatomic potential is most crucial for model formulation. The simplest potentials to use are pair potentials such as the Lennard-Jones or Morse potentials, but improved accuracy is obtained by considering three-body potentials such as the Tersoff–Brenner potential of Eq. (2.2), thus accounting for changes in bond angles as well as bond lengths (see Fig. 2).

We propose another approach to help account for the simultaneous multi-body interactions (see also Volokh, 2004; Volokh and Gao, 2005). We assume that the simultaneous multi-body interactions are related with the change of the interbond angles, which themselves are a result of the distortion of the atomic lattice. Thus, the deformation of the lattice can be decomposed into a self-similar deformation, which does not lead to the change of the interbond angles, and a distortional deformation, which does lead to the change of the interbond angles (Fig. 3). Now the length of every atomic bond is generally changed due to both the self-similar (spherical) and bond-angle-changing (distortional) lattice deformation. Such a split of the bond length can be accomplished by means of the spherical–deviatoric decomposition of the Green strain tensor. After the split, the continuum-atomistic potential can be written as a function of the two changes in bond length independently. The latter will allow for preserving the simple structure of the interatomic potentials while accounting to some degree for the multi-body effects. We accomplish this as follows.

From the point of view of continuum mechanics, it is convenient to use a quadratic measure of the interatomic distance change
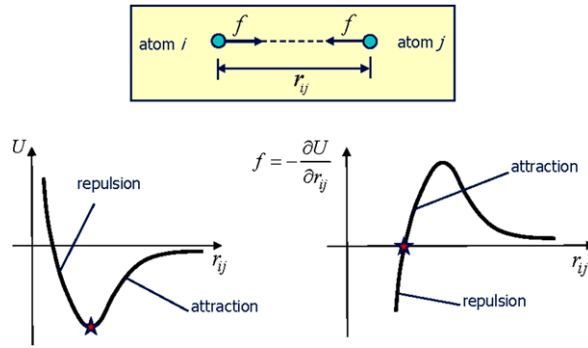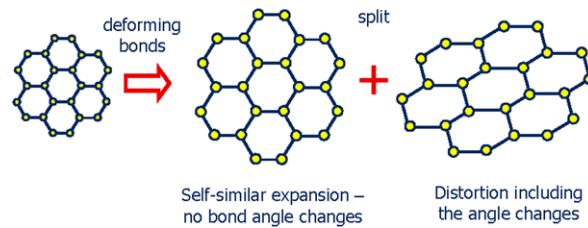
Fig. 2. Pair interatomic potential.



Fig. 3. Split of the bond length in the stretching (self-similar deformation) and the bending (distortional deformation).

$$\Delta = l^2 - L^2, \tag{2.21}$$

where

$$l = r_{ij} = L\sqrt{\boldsymbol{\xi} \cdot (\mathbf{1} + 2\mathbf{E})\boldsymbol{\xi}}, \quad L = R_{ij} = \sqrt{\mathbf{R}_{ij} \cdot \mathbf{R}_{ij}}, \quad \boldsymbol{\xi} = \mathbf{R}_{ij}/L. \tag{2.22}$$

Substituting Eq. (2.22) in Eq. (2.21), we have

$$\Delta = 2L^2 \boldsymbol{\xi} \cdot \mathbf{E}\boldsymbol{\xi}, \tag{2.23}$$

Let the Green strain tensor be decomposed into spherical and deviatoric parts accordingly

$$\mathbf{E} = \frac{1}{3}(\text{tr}\,\mathbf{E})\mathbf{1} + \hat{\mathbf{E}}. \tag{2.24}$$

Substituting Eq. (2.24) in Eq. (2.23), we have

$$\Delta = \psi + \hat{\Delta}, \tag{2.25}$$

where

$$\psi = \frac{2}{3}L^2 \text{tr}\,\mathbf{E}, \tag{2.26}$$

$$\hat{\Delta} = 2L^2 \boldsymbol{\xi} \cdot \hat{\mathbf{E}}\boldsymbol{\xi}. \tag{2.27}$$

Here $\psi$ designates the squared bond length change due to the self-similar lattice stretch and $\hat{\Delta}$ designates the squared bond length change due to the lattice distortion. The former is driven by the spherical deformation and the latter is driven by the deviatoric deformation.

Now we can write the energy density as follows:

$$W = \langle U(\psi, \hat{\Delta}) \rangle = W(\mathbf{E}), \tag{2.28}$$

where the brackets mean the finite sum average as in Eq. (2.10) or the integral average as in Eq. (2.20).

Substituting Eq. (2.28) in Eqs. (2.14) and (2.15), we have

$$\mathbf{S} = \left\langle \frac{2L^2}{3}(U_\psi - U_{\hat{A}})\mathbf{1} + 2L^2 U_{\hat{A}}\boldsymbol{\xi} \otimes \boldsymbol{\xi} \right\rangle, \tag{2.29}$$

$$\mathbf{C} = \left\langle \frac{4L^4}{9}(U_{\psi\psi} + U_{\hat{A}\hat{A}} - 2U_{\psi\hat{A}})\mathbf{1} \otimes \mathbf{1} + 4L^4 U_{\hat{A}\hat{A}}\boldsymbol{\xi} \otimes \boldsymbol{\xi} \otimes \boldsymbol{\xi} \otimes \boldsymbol{\xi} + \frac{4L^4}{3}(U_{\psi\hat{A}} - U_{\hat{A}\hat{A}})(\boldsymbol{\xi} \otimes \boldsymbol{\xi} \otimes \mathbf{1} + \mathbf{1} \otimes \boldsymbol{\xi} \otimes \boldsymbol{\xi}) \right\rangle, \tag{2.30}$$

where the following results were accounted for

$$\frac{\partial \psi}{\partial \mathbf{E}} = \frac{2L^2}{3}\mathbf{1}, \quad \frac{\partial \hat{A}}{\partial \mathbf{E}} = 2L^2\boldsymbol{\xi} \otimes \boldsymbol{\xi} - \frac{2L^2}{3}\mathbf{1}, \quad \frac{\partial^2 \psi}{\partial \mathbf{E}\partial \mathbf{E}} = \mathbf{0} = \frac{\partial^2 \hat{A}}{\partial \mathbf{E}\,\partial \mathbf{E}}. \tag{2.31}$$

To connect the continuum and atomistic problems, we must identify the potential to be used. Using the Tersoff–Brenner potential of Eq. (2.2) as a basis, we write our potential as

$$U(\psi, \hat{A}) = \frac{D}{S-1}\left\{ \exp\left[ -\sqrt{2S}\beta\left( \sqrt{\psi + f\hat{A} + L^2} - L \right) \right] - S\exp\left[ -\sqrt{2/S}\beta\left( \sqrt{\psi + f\hat{A} + L^2} - L \right) \right] \right\}, \tag{2.32}$$

where the cutoff function (2.5) has been ignored and the three-body coupling functions (2.6) have been set equal to one. We wish to emphasize that we are not neglecting the multi-body interaction in this approach, although we are not using the atomistic version of this coupling in the Brenner potential. Instead, we are incorporating the multi-body interaction (without limiting the number of atoms involved in the interaction) directly into the continuum atomistic potential represented by Eq. (2.32).

This split continuum-atomistic potential (2.32) has one unknown dimensionless coefficient $f$ related with the lattice distortion, i.e. the bond bending. This coefficient can be determined either through comparison with experimental results or through theoretical analysis as follows.

Some experimental research groups have estimated the Poisson ratio of carbon nanotubes assuming isotropy of the CNT structure (this assumption is obviously idealization for single-walled CNTs, which have a pronounced crystalline structure). Single-walled CNTs can be considered as *isotropic for small strains* (see results below). Based on the value of the Poisson ratio we can derive the value for the parameter $f$ of the continuum-atomistic potential (2.32). We begin by linearizing the constitutive law about $\psi = 0$ and $\hat{A} = 0$:

$$\begin{cases} U_{\hat{A}\hat{A}} = f^2 U_{\psi\psi}, \\ U_{\psi\hat{A}} = f U_{\psi\psi}. \end{cases} \tag{2.33}$$

In this case, the initial tangent moduli (designated with superscript zero) take the following form

$$C^0_{IJMN} = \left\langle \frac{4L^4}{9}U_{\psi\psi}\left\{ (1-f)^2\delta_{IJ}\delta_{MN} + 9f^2\xi_I\xi_J\xi_M\xi_N + 3f(1-f)(\xi_I\xi_J\delta_{MN} + \delta_{IJ}\xi_M\xi_N) \right\} \right\rangle. \tag{2.34}$$

The brackets mean

$$\langle \bullet \rangle = \frac{1}{V_0} \int_{-\pi}^{\pi} \int_0^{\pi} \int_L \bullet D_L \sin\theta \, dL \, d\theta \, d\varphi, \tag{2.35}$$

where we have used Eq. (2.20) with $D_V(L, \theta, \varphi) = D_L(L)$ because of isotropy. Since we have the geometric results

$$\int_{-\pi}^{\pi} \int_0^{\pi} \xi_I\xi_J\xi_M\xi_N \sin\theta \, d\theta \, d\varphi = \frac{4\pi}{15}(\delta_{IJ}\delta_{MN} + \delta_{IM}\delta_{JN} + \delta_{IN}\delta_{JM}), \tag{2.36}$$

$$\int_{-\pi}^{\pi} \int_0^{\pi} \xi_I\xi_J \sin\theta \, d\theta \, d\varphi = \frac{4\pi}{3}\delta_{IJ}, \tag{2.37}$$

$$\int_{-\pi}^{\pi} \int_0^{\pi} \sin\theta \, d\theta \, d\varphi = 4\pi, \tag{2.38}$$

we can compute the right-hand side of Eq. (2.34) to give

$$C^0_{IJMN} = U_{\psi\psi}\pi\langle L^4\rangle \left\{ \left(\frac{16}{9} - \frac{32}{45}f^2\right)\delta_{IJ}\delta_{MN} + \frac{16}{15}f^2(\delta_{IM}\delta_{JN} + \delta_{IN}\delta_{JM}) \right\}. \tag{2.39}$$

Eq. (2.39) essentially states that the Lame parameters of isotropic elasticity have the following expressions

$$\lambda = U_{\psi\psi}\pi\langle L^4\rangle_L \left(\frac{16}{9} - \frac{32}{45}f^2\right), \tag{2.40}$$

$$\mu = U_{\psi\psi}\pi\langle L^4\rangle_L \frac{16}{15}f^2. \tag{2.41}$$

The relationship between the Lame parameters and the Poisson ratio is

$$\lambda = 2\mu v/(1 - 2v). \tag{2.42}$$

Reich et al. (2004) estimated the Poisson ratio $v = 0.14$ from their experiments. Substituting Eqs. (2.40) and (2.41) in Eq. (2.42) and setting $v = 0.14$, we obtain

$$f \cong 1.26. \tag{2.43}$$

A theoretical estimate of the magnitude of $f$ can be obtained by linking the potentials (2.2) and (2.32) through the following formal procedure. Consider the following imaginary deformation of an infinite graphite sheet shown in Fig. 4a

$$\mathbf{F} = \lambda_1\mathbf{k}_1 \otimes \mathbf{K}_1 + \mathbf{k}_2 \otimes \mathbf{K}_2 + \mathbf{k}_3 \otimes \mathbf{K}_3, \tag{2.44}$$

where $\mathbf{k}_i$ and $\mathbf{K}_I$ are the coinciding Cartesian base vectors related with current and referential configurations accordingly.

We substitute this deformation in the empirical potentials (2.2) and (2.32) by using the Cauchy–Born rule (2.8). Now, the strain energy density based on the Tersoff–Brenner potential (2.2) is a function of the axial stretch $\lambda_1$ only – $W^{TB}(\lambda_1)$. On the other hand, the strain energy based on the potential presented in this work (2.32) is a function of both $\lambda_1$ and $f - W(\lambda_1, f)$. In order to find $f$ we equate the second derivatives of both strain energies at $\lambda_1 = 1$, i.e. we define the equivalent initial stiffness

$$\frac{\partial^2 W^{TB}}{\partial\lambda_1^2}(\lambda_1 = 1) = \frac{\partial^2 W}{\partial\lambda_1^2}(\lambda_1 = 1, f). \tag{2.45}$$

This is a transcendent equation with respect to $f$, which can be solved numerically. The solution is

$$f \cong 1.24. \tag{2.46}$$

Alternatively, we define the uniaxial stretch in the orthogonal direction (Fig. 4b)

$$\mathbf{F} = \mathbf{k}_1 \otimes \mathbf{K}_1 + \lambda_2\mathbf{k}_2 \otimes \mathbf{K}_2 + \mathbf{k}_3 \otimes \mathbf{K}_3, \tag{2.47}$$
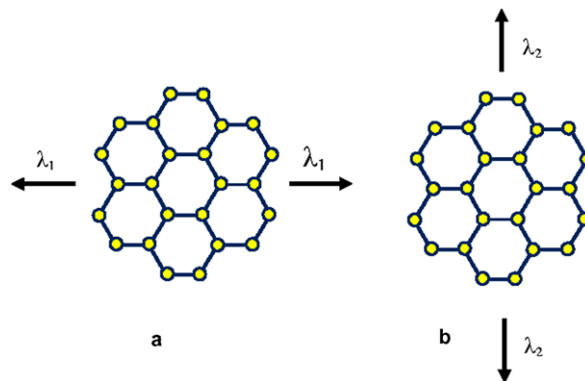
and use the equivalence condition



Fig. 4. Imaginary deformations (given by Eqs. (2.44) and (2.47)) for comparison of the potentials given by Eqs. (2.2) and (2.32).

$$\frac{\partial^2 W^{\mathrm{TB}}}{\partial \lambda_2^2}(\lambda_2 = 1) = \frac{\partial^2 W}{\partial \lambda_2^2}(\lambda_2 = 1, f). \tag{2.48}$$

The solution for parameter $f$ is again 1.24, as in Eq. (2.46). It is remarkable that

$$\frac{\partial^2 W^{\mathrm{TB}}}{\partial \lambda_1^2}(\lambda_1 = 1) = \frac{\partial^2 W^{\mathrm{TB}}}{\partial \lambda_2^2}(\lambda_2 = 1), \tag{2.49}$$

i.e. the hexagonal sheet of the material can be considered isotropic under small initial deformations.

The magnitude of parameter $f$ given by Eq. (2.46) practically coincides with the magnitude of $f$ given by Eq. (2.43). This result is encouraging.

## 3. Single wall carbon nanotubes under tension

In this section, we will use the developed continuum-atomistic theory to assess the tensile strength of the single wall zigzag and armchair nanotubes. First, we develop equations describing the pre-bifurcation state of the nanotubes (Section 3.1). Then we analyze the bifurcation (Section 3.2). Finally, we discuss the results of the analysis (Section 3.3).

### 3.1. Pre-bifurcation state

Adopting a Lagrangian (referential) description, the equilibrium equations without the body forces take the form

$$\mathrm{Div}\,\mathbf{P} = \mathbf{0}, \tag{3.1}$$

where

$$\mathbf{P} = \mathbf{FS} \tag{3.2}$$

is the first (two-point) Piola–Kirchhoff stress tensor; $\mathbf{S} = \mathbf{S}^{\mathrm{T}}$ is the second (symmetric) Piola–Kirchhoff stress tensor obtained from Eq. (2.14).

The boundary conditions are

$$\begin{cases} \boldsymbol{\chi} = \bar{\boldsymbol{\chi}} & \text{on } \partial\Omega_{\boldsymbol{\chi}}, \\ \mathbf{Pn} = \bar{\mathbf{t}} & \text{on } \partial\Omega_{\mathbf{t}}, \end{cases} \tag{3.3}$$

where $\mathbf{t}$ is the surface traction per unit reference area; $\mathbf{n}$ is a unit outward normal to the reference surface; and the barred quantities are prescribed.

We will consider governing equations directly with respect to the following referential and current *ortho-normal bases* in cylindrical coordinates $\{R, \Theta, Z\}$ and $\{r, \theta, z\}$

$$\begin{cases} \mathbf{K}_R(\Theta) = (\cos\Theta, \sin\Theta, 0)^{\mathrm{T}} & \mathbf{K}_{\Theta}(\Theta) = (-\sin\Theta, \cos\Theta, 0)^{\mathrm{T}} & \mathbf{K}_Z = (0, 0, 1)^{\mathrm{T}}, \\ \mathbf{k}_r(\theta) = (\cos\theta, \sin\theta, 0)^{\mathrm{T}} & \mathbf{k}_{\theta}(\theta) = (-\sin\theta, \cos\theta, 0)^{\mathrm{T}} & \mathbf{k}_z = (0, 0, 1)^{\mathrm{T}}. \end{cases} \tag{3.4}$$

In this case, the current position vector of particle $\mathbf{X}$ has the following general representation

$$\boldsymbol{\chi}(\mathbf{X}) = r\mathbf{k}_r(\theta) + z\mathbf{k}_z, \tag{3.5}$$

where $\{r, \theta, z\}$ are functions of $\{R, \Theta, Z\}$.

Carbon nanotubes are very thin because they include only one or very few atomic layers. Based on this notion we ignore variation of all quantities with respect to $R$, which is the initial tube radius (see also Remark 3 at the end of Section 2.2). We assume that the pre-bifurcation state is an axisymmetric tension, which can be described as follows:

$$r = r(\alpha), \quad \theta = \Theta, \quad z = \alpha Z, \tag{3.6}$$

where $r$ is the current tube radius, which does not depend on $R$, and the axial stretch $\alpha$ is the control parameter.

Substituting Eq. (3.6) in Eqs. (3.4) and (3.5), we have

$$\mathbf{k}_r(\theta) = \mathbf{k}_r(\Theta) = \mathbf{K}_R(\Theta), \quad \mathbf{k}_\theta(\theta) = \mathbf{k}_\theta(\Theta) = \mathbf{K}_\Theta(\Theta), \quad \mathbf{k}_z = \mathbf{K}_Z, \tag{3.7}$$

$$\boldsymbol{\chi}(\mathbf{X}) = r\mathbf{k}_r(\Theta) + \alpha Z\mathbf{k}_z. \tag{3.8}$$

The coincidence of the base vectors in the current and referential configurations for $\theta = \Theta$ leads to dramatic simplifications of all subsequent equations. In principle, we can abandon the use of $\mathbf{k}_r(\Theta)$, $\mathbf{k}_\theta(\Theta)$, $\mathbf{k}_z$ replacing them with $\mathbf{K}_R(\Theta)$, $\mathbf{K}_\Theta(\Theta)$, $\mathbf{K}_Z$. However, we retain them in order to emphasize the two-point character of the deformation gradient tensor:

$$\mathbf{F} = \frac{\partial\boldsymbol{\chi}(\mathbf{X})}{\partial R} \otimes \mathbf{K}_R(\Theta) + \frac{\partial\boldsymbol{\chi}(\mathbf{X})}{R\partial\Theta} \otimes \mathbf{K}_\Theta(\Theta) + \frac{\partial\boldsymbol{\chi}(\mathbf{X})}{\partial Z} \otimes \mathbf{K}_Z = \frac{r}{R}\mathbf{k}_\theta(\Theta) \otimes \mathbf{K}_\Theta(\Theta) + \alpha\mathbf{k}_z \otimes \mathbf{K}_Z, \tag{3.9}$$

where the relation $\partial\mathbf{k}_r(\Theta)/\partial\Theta = \mathbf{k}_\theta(\Theta)$ has been used. Henceforth we suppress the argument of the base vectors.

Then we have from Eq. (3.2)

$$\mathbf{P} = \frac{r}{R} S_{\Theta R}\mathbf{k}_\theta \otimes \mathbf{K}_R + \frac{r}{R} S_{\Theta\Theta}\mathbf{k}_\theta \otimes \mathbf{K}_\Theta + \frac{r}{R} S_{\Theta Z}\mathbf{k}_\theta \otimes \mathbf{K}_Z + \alpha S_{ZR}\mathbf{k}_z \otimes \mathbf{K}_R + \alpha S_{Z\Theta}\mathbf{k}_z \otimes \mathbf{K}_\Theta + \alpha S_{ZZ}\mathbf{k}_z \otimes \mathbf{K}_Z. \tag{3.10}$$

Substituting Eq. (3.10) in Eq. (3.1), we get the following equilibrium equation

$$\mathrm{Div}\,\mathbf{P} = -\frac{r}{R^2} S_{\Theta\Theta}\mathbf{k}_r + \left(\frac{r}{R^2} S_{\Theta R} + \frac{r}{R^2}\frac{\partial S_{\Theta\Theta}}{\partial\Theta} + \frac{r}{R}\frac{\partial S_{\Theta Z}}{\partial Z}\right)\mathbf{k}_\theta + \left(\frac{\alpha}{R} S_{ZR} + \frac{\alpha}{R}\frac{\partial S_{Z\Theta}}{\partial\Theta} + \alpha\frac{\partial S_{ZZ}}{\partial Z}\right)\mathbf{k}_z = \mathbf{0}, \tag{3.11}$$

where the following derivatives of the base vectors were used

$$\frac{\partial\mathbf{K}_R}{\partial\Theta} = \mathbf{K}_\Theta = \mathbf{k}_\theta = \frac{\partial\mathbf{k}_r}{\partial\Theta}, \quad \frac{\partial\mathbf{K}_\Theta}{\partial\Theta} = -\mathbf{K}_R = -\mathbf{k}_r = \frac{\partial\mathbf{k}_\theta}{\partial\Theta}. \tag{3.12}$$

Note that equilibrium equation (3.11) can be interpreted as the average over the wall thickness if all terms are pre-multiplied by the thickness magnitude, i.e. integrated over the thickness. Evidently, this will not affect the subsequent analysis and we omit the wall thickness in the subsequent reasoning.

Assume now that the lateral surface of the CNT is stress-free

$$\mathbf{P}\mathbf{K}_R = \frac{r}{R} S_{\Theta R}\mathbf{k}_\theta + \alpha S_{ZR}\mathbf{k}_z = \mathbf{0}. \tag{3.13}$$

This means

$$S_{\Theta R} = 0, \quad S_{ZR} = 0. \tag{3.14}$$

Substituting Eq. (3.14) into Eq. (3.11), we obtain

$$S_{\Theta\Theta} = 0, \quad \frac{\partial S_{\Theta Z}}{\partial Z} = 0, \quad \frac{\partial S_{Z\Theta}}{R\partial\Theta} + \frac{\partial S_{ZZ}}{\partial Z} = 0. \tag{3.15}$$

We assume that there are no tangent tractions at the edges $Z = 0, H$ of the CNT

$$\mathbf{k}_\theta \cdot \mathbf{P}\mathbf{K}_Z = \frac{r}{R} S_{\Theta Z} = 0. \tag{3.16}$$

We conclude from Eq. (3.15$_2$) and boundary condition (3.16) that $S_{\Theta Z}$ does not depend on $Z$. Enforcing axial symmetry we conclude that $S_{\Theta Z}$ vanishes while $S_{ZZ}$ is constant.

In summary, the final radius $r$ of the CNT can be found from Eqs. (3.15$_1$) and (2.29) by solving

$$S_{\Theta\Theta} = \left\langle \frac{2L^2}{3}\left(U_\psi - U_{\hat{\Lambda}} + 3U_{\hat{\Lambda}}\xi_\Theta^2\right)\right\rangle = 0. \tag{3.17}$$

The axial stress for the given axial stretch $\alpha$ is computed from

$$S_{ZZ} = \left\langle \frac{2L^2}{3}\left(U_\psi - U_{\hat{\Lambda}} + 3U_{\hat{\Lambda}}\xi_Z^2\right)\right\rangle. \tag{3.18}$$

Eqs. (3.17) and (3.18) include the dependence on $\psi$ and $\hat{\Delta}$ which take the form

$$\psi = \frac{2}{3}L^2(E_{\Theta\Theta} + E_{ZZ}), \tag{3.19}$$

$$\hat{\Delta} = 2L^2(E_{\Theta\Theta}(\xi_\Theta^2 - 1/3) + E_{ZZ}(\xi_Z^2 - 1/3)), \tag{3.20}$$

where $E_{\Theta\Theta} = (r^2/R^2 - 1)/2$ and $E_{ZZ} = (\alpha^2 - 1)/2$.

## 3.2. Bifurcation state

In order to formulate the bifurcation problem we superimpose small perturbing displacements

$$\mathbf{u} = u_r\mathbf{k}_r + u_\theta\mathbf{k}_\theta + u_z\mathbf{k}_z \tag{3.21}$$

on the current stress/deformation state. In this case, we have the following perturbed equilibrium equation instead of Eq. (3.1)

$$\text{Div}\,\widetilde{\mathbf{P}} = \mathbf{0}, \tag{3.22}$$

and the following boundary conditions instead of Eq. (3.3), assuming 'dead' surface tractions and displacements,

$$\begin{cases} \mathbf{u} = \mathbf{0} & \text{on } \partial\Omega_\chi, \\ \widetilde{\mathbf{P}}\mathbf{n} = \mathbf{0} & \text{on } \partial\Omega_{\mathbf{t}}. \end{cases} \tag{3.23}$$

Here we have

$$\widetilde{\mathbf{P}} = \widetilde{\mathbf{F}}\mathbf{S} + \mathbf{F}\widetilde{\mathbf{S}}, \quad \widetilde{\mathbf{F}} = \partial\mathbf{u}/\partial\mathbf{X}, \quad \widetilde{\mathbf{S}} = \mathbf{C} : \widetilde{\mathbf{E}}, \quad \widetilde{\mathbf{E}} = (\widetilde{\mathbf{F}}^{\mathrm{T}}\mathbf{F} + \mathbf{F}^{\mathrm{T}}\widetilde{\mathbf{F}})/2, \tag{3.24}$$

with all perturbed solutions designated with a tilde.

In the specific case under consideration we have

$$\begin{aligned}
\widetilde{\mathbf{F}} &= \frac{\partial\mathbf{u}}{\partial\mathbf{X}} \\
&= \left(\frac{\partial u_r}{R\partial\Theta} - \frac{u_\theta}{R}\right)\mathbf{k}_r \otimes \mathbf{K}_\Theta + \frac{\partial u_r}{\partial Z}\mathbf{k}_r \otimes \mathbf{K}_Z + \left(\frac{\partial u_\theta}{R\partial\Theta} + \frac{u_r}{R}\right)\mathbf{k}_\theta \otimes \mathbf{K}_\Theta + \frac{\partial u_\theta}{\partial Z}\mathbf{k}_\theta \otimes \mathbf{K}_Z + \frac{\partial u_z}{R\partial\Theta}\mathbf{k}_z \otimes \mathbf{K}_\Theta \\
&\quad + \frac{\partial u_z}{\partial Z}\mathbf{k}_z \otimes \mathbf{K}_Z, \tag{3.25}
\end{aligned}$$

$$\mathbf{S} = S_{ZZ}\mathbf{K}_Z \otimes \mathbf{K}_Z, \tag{3.26}$$

$$\widetilde{\mathbf{F}}\mathbf{S} = S_{ZZ}\frac{\partial u_r}{\partial Z}\mathbf{k}_r \otimes \mathbf{K}_Z + S_{ZZ}\frac{\partial u_\theta}{\partial Z}\mathbf{k}_\theta \otimes \mathbf{K}_Z + S_{ZZ}\frac{\partial u_z}{\partial Z}\mathbf{k}_z \otimes \mathbf{K}_Z, \tag{3.27}$$

$$\mathbf{F} = \frac{r}{R}\mathbf{k}_\theta \otimes \mathbf{K}_\Theta + \alpha\mathbf{k}_z \otimes \mathbf{K}_Z, \tag{3.28}$$

$$\begin{aligned}
\widetilde{\mathbf{E}} &= \frac{r}{R}\left(\frac{\partial u_\theta}{R\partial\Theta} + \frac{u_r}{R}\right)\mathbf{K}_\Theta \otimes \mathbf{K}_\Theta + \frac{1}{2}\left(\frac{r}{R}\frac{\partial u_\theta}{\partial Z} + \alpha\frac{\partial u_z}{R\partial\Theta}\right)\mathbf{K}_\Theta \otimes \mathbf{K}_Z + \frac{1}{2}\left(\frac{r}{R}\frac{\partial u_\theta}{\partial Z} + \alpha\frac{\partial u_z}{R\partial\Theta}\right)\mathbf{K}_Z \otimes \mathbf{K}_\Theta \\
&\quad + \alpha\frac{\partial u_z}{\partial Z}\mathbf{K}_Z \otimes \mathbf{K}_Z, \tag{3.29}
\end{aligned}$$

$$\widetilde{\mathbf{S}} = C_{IJ\Theta\Theta}\frac{r}{R}\left(\frac{\partial u_\theta}{R\partial\Theta} + \frac{u_r}{R}\right)\mathbf{K}_I \otimes \mathbf{K}_J + C_{IJ\Theta Z}\left(\frac{r}{R}\frac{\partial u_\theta}{\partial Z} + \alpha\frac{\partial u_z}{R\partial\Theta}\right)\mathbf{K}_I \otimes \mathbf{K}_J + C_{IJZZ}\alpha\frac{\partial u_z}{\partial Z}\mathbf{K}_Z \otimes \mathbf{K}_Z, \tag{3.30}$$

where $\Theta \equiv 2$, or $Z \equiv 3$ are fixed indices and no summation over them is supposed.

Then we have

$$\mathbf{F}\widetilde{\mathbf{S}} = \left( C_{\Theta J \Theta \Theta} \frac{r^2}{R^2} \left( \frac{\partial u_\theta}{R \partial \Theta} + \frac{u_r}{R} \right) + C_{\Theta J \Theta Z} \frac{r}{R} \left( \frac{r}{R} \frac{\partial u_\theta}{\partial Z} + \alpha \frac{\partial u_z}{R \partial \Theta} \right) + C_{\Theta J Z Z} \alpha \frac{r}{R} \frac{\partial u_z}{\partial Z} \right) \mathbf{k}_\theta \otimes \mathbf{K}_J$$
$$+ \left( C_{ZJ\Theta\Theta} \alpha \frac{r}{R} \left( \frac{\partial u_\theta}{R \partial \Theta} + \frac{u_r}{R} \right) + C_{ZJ\Theta Z} \alpha \left( \frac{r}{R} \frac{\partial u_\theta}{\partial Z} + \alpha \frac{\partial u_z}{R \partial \Theta} \right) + C_{ZJZZ} \alpha^2 \frac{\partial u_z}{\partial Z} \right) \mathbf{k}_z \otimes \mathbf{K}_J, \tag{3.31}$$

where index $J$ is equal to $\Theta$ or $Z$.

Substituting Eqs. (3.27) and (3.31) in Eq. (3.24$_1$) we obtain the following increment of the first Piola–Kirchhoff stress

$$\widetilde{\mathbf{P}} = \widetilde{P}_{rZ} \mathbf{k}_r \otimes \mathbf{K}_Z + \widetilde{P}_{\theta\Theta} \mathbf{k}_\theta \otimes \mathbf{K}_\Theta + \widetilde{P}_{\theta Z} \mathbf{k}_\theta \otimes \mathbf{K}_Z + \widetilde{P}_{z\Theta} \mathbf{k}_z \otimes \mathbf{K}_\Theta + \widetilde{P}_{zZ} \mathbf{k}_z \otimes \mathbf{K}_Z, \tag{3.32}$$

$$\begin{cases}
\widetilde{P}_{rZ} = S_{ZZ} \dfrac{\partial u_r}{\partial Z}, \\[2mm]
\widetilde{P}_{\theta\Theta} = C_{\Theta\Theta\Theta\Theta} \dfrac{r^2}{R^3} \left( \dfrac{\partial u_\theta}{\partial \Theta} + u_r \right) + C_{\Theta\Theta\Theta Z} \left( \dfrac{r^2}{R^2} \dfrac{\partial u_\theta}{\partial Z} + \alpha \dfrac{r \partial u_z}{R^2 \partial \Theta} \right) + C_{\Theta\Theta ZZ} \alpha \dfrac{r}{R} \dfrac{\partial u_z}{\partial Z}, \\[2mm]
\widetilde{P}_{\theta Z} = C_{\Theta Z\Theta\Theta} \dfrac{r^2}{R^3} \left( \dfrac{\partial u_\theta}{\partial \Theta} + u_r \right) + C_{\Theta Z\Theta Z} \left( \dfrac{r^2}{R^2} \dfrac{\partial u_\theta}{\partial Z} + \alpha \dfrac{r \partial u_z}{R^2 \partial \Theta} \right) + C_{\Theta ZZZ} \alpha \dfrac{r}{R} \dfrac{\partial u_z}{\partial Z} + S_{ZZ} \dfrac{\partial u_\theta}{\partial Z}, \\[2mm]
\widetilde{P}_{z\Theta} = \alpha C_{\Theta Z\Theta\Theta} \dfrac{r}{R^2} \left( \dfrac{\partial u_\theta}{\partial \Theta} + u_r \right) + C_{\Theta Z\Theta Z} \left( \alpha \dfrac{r}{R} \dfrac{\partial u_\theta}{\partial Z} + \alpha^2 \dfrac{\partial u_z}{R \partial \Theta} \right) + C_{\Theta ZZZ} \alpha^2 \dfrac{\partial u_z}{\partial Z}, \\[2mm]
\widetilde{P}_{zZ} = \alpha C_{ZZ\Theta\Theta} \dfrac{r}{R^2} \left( \dfrac{\partial u_\theta}{\partial \Theta} + u_r \right) + C_{ZZ\Theta Z} \left( \alpha \dfrac{r}{R} \dfrac{\partial u_\theta}{\partial Z} + \alpha^2 \dfrac{\partial u_z}{R \partial \Theta} \right) + C_{ZZZZ} \alpha^2 \dfrac{\partial u_z}{\partial Z} + S_{ZZ} \dfrac{\partial u_z}{\partial Z},
\end{cases} \tag{3.33}$$

Substituting Eq. (3.32) in Eq. (3.22), we get the following perturbed equilibrium equations

$$\mathrm{Div}\, \widetilde{\mathbf{P}} = \left( \frac{\partial \widetilde{P}_{rZ}}{\partial Z} - \frac{\widetilde{P}_{\theta\Theta}}{R} \right) \mathbf{k}_r + \left( \frac{\partial \widetilde{P}_{\theta Z}}{\partial Z} + \frac{\partial \widetilde{P}_{\theta\Theta}}{R \partial \Theta} \right) \mathbf{k}_\theta + \left( \frac{\partial \widetilde{P}_{z\Theta}}{R \partial \Theta} + \frac{\partial \widetilde{P}_{zZ}}{\partial Z} \right) \mathbf{k}_z = \mathbf{0}. \tag{3.34}$$

Substituting Eq. (3.33) in Eq. (3.34), we obtain the following homogeneous system of equations

$$\begin{cases}
L_{rr} u_r + L_{r\theta} u_\theta + L_{rz} u_z = 0, \\
L_{\theta r} u_r + L_{\theta\theta} u_\theta + L_{\theta z} u_z = 0, \\
L_{zr} u_r + L_{z\theta} u_\theta + L_{zz} u_z = 0,
\end{cases} \tag{3.35}$$

where

$$\begin{cases}
L_{rr} = S_{ZZ} \dfrac{\partial^2}{\partial Z^2} - C_{\Theta\Theta\Theta\Theta} \dfrac{r^2}{R^4}, \\[2mm]
L_{r\theta} = -C_{\Theta\Theta\Theta\Theta} \dfrac{r^2}{R^4} \dfrac{\partial}{\partial \Theta}, \\[2mm]
L_{rz} = -C_{\Theta\Theta ZZ} \dfrac{\alpha r}{R^2} \dfrac{\partial}{\partial Z}, \\[2mm]
L_{\theta r} = C_{\Theta\Theta\Theta\Theta} \dfrac{r^2}{R^4} \dfrac{\partial}{\partial \Theta}, \\[2mm]
L_{\theta\theta} = \left( C_{\Theta Z\Theta Z} \dfrac{r^2}{R^2} + S_{ZZ} \right) \dfrac{\partial^2}{\partial Z^2} + C_{\Theta\Theta\Theta\Theta} \dfrac{r^2}{R^4} \dfrac{\partial^2}{\partial \Theta^2}, \\[2mm]
L_{\theta z} = (C_{\Theta Z\Theta Z} + C_{\Theta\Theta ZZ}) \dfrac{\alpha r}{R^2} \dfrac{\partial^2}{\partial \Theta \partial Z}, \\[2mm]
L_{zr} = C_{\Theta\Theta ZZ} \dfrac{\alpha r}{R^2} \dfrac{\partial}{\partial Z}, \\[2mm]
L_{z\theta} = (C_{\Theta Z\Theta Z} + C_{\Theta\Theta ZZ}) \dfrac{\alpha r}{R^2} \dfrac{\partial^2}{\partial Z \partial \Theta}, \\[2mm]
L_{zz} = C_{\Theta Z\Theta Z} \dfrac{\alpha^2}{R^2} \dfrac{\partial^2}{\partial \Theta^2} + \left( C_{ZZZZ} \alpha^2 + S_{ZZ} \right) \dfrac{\partial^2}{\partial Z^2}.
\end{cases} \tag{3.36}$$

The incremental boundary conditions at $Z = 0, H$ take the form

$$u_z = 0, \quad \widetilde{P}_{rZ} = S_{ZZ}\frac{\partial u_r}{\partial Z} = 0, \quad \widetilde{P}_{\theta Z} = \left(C_{\Theta Z\Theta Z}\frac{r^2}{R^2} + S_{ZZ}\right)\frac{\partial u_\theta}{\partial Z} + \alpha C_{\Theta Z\Theta Z}\frac{r\partial u_z}{R^2\partial\Theta} = 0. \quad (3.37)$$

Note we have set the tangent moduli $C_{\Theta ZZZ} = C_{ZZ\Theta Z}$, $C_{\Theta\Theta\Theta Z} = C_{\Theta Z\Theta\Theta}$ equal to zero independently of the deformation because of the symmetry properties of the armchair and zigzag nanotubes. The nonzero tangent moduli are computed as follows:

$$\begin{cases} C_{\Theta\Theta\Theta\Theta} = \left\langle \dfrac{4L^4}{9}(U_{\psi\psi} + U_{\hat{A}\hat{A}}(1 - 3\xi_\Theta^2)^2 + 2(3\xi_\Theta^2 - 1)U_{\psi\hat{A}}\right\rangle, \\[2mm] C_{ZZZZ} = \left\langle \dfrac{4L^4}{9}(U_{\psi\psi} + U_{\hat{A}\hat{A}}(1 - 3\xi_Z^2)^2 + 2(3\xi_Z^2 - 1)U_{\psi\hat{A}}\right\rangle, \\[2mm] C_{\Theta Z\Theta Z} = \left\langle 4L^4 U_{\hat{A}\hat{A}}\xi_Z^2\xi_\Theta^2\right\rangle, \\[2mm] C_{\Theta\Theta ZZ} = \left\langle \dfrac{4L^4}{9}(U_{\psi\psi} + U_{\hat{A}\hat{A}}(9\xi_\Theta^2\xi_Z^2 - 2) + U_{\psi\hat{A}}\right\rangle. \end{cases} \quad (3.38)$$

Since $\boldsymbol{\xi} = \cos\phi\mathbf{K}_\Theta + \sin\phi\mathbf{K}_Z$, we have

$$\xi_\Theta^2 = \cos^2\phi, \quad \xi_Z^2 = \sin^2\phi, \quad (3.39)$$

where $\phi$ is the angle between the bond $i$–$j$ and axis $Z$.

We consider solutions of Eq. (3.35) in the form of trigonometric series

$$\begin{cases} u_r = u_r^{(m,n)}\cos(n\Theta)\cos(m\pi Z/H), \\ u_\theta = u_\theta^{(m,n)}\sin(n\Theta)\cos(m\pi Z/H), \\ u_z = u_z^{(m,n)}\cos(n\Theta)\sin(m\pi Z/H). \end{cases} \quad (3.40)$$

These expressions obey boundary conditions (3.37), and a nontrivial solution of Eq. (3.35) is obtained under condition

$$\det \boldsymbol{\Lambda} = 0, \quad (3.41)$$

where the entries of matrix $\boldsymbol{\Lambda}$ are

$$\begin{cases} \Lambda_{11} = -S_{ZZ}(m\pi/H)^2 - C_{\Theta\Theta\Theta\Theta}r^2/R^4, \\ \Lambda_{12} = \Lambda_{21} = -C_{\Theta\Theta\Theta\Theta}nr^2/R^4, \\ \Lambda_{13} = \Lambda_{31} = -C_{\Theta\Theta ZZ}(m\pi/H)\alpha r/R^2, \\ \Lambda_{22} = -(C_{\Theta Z\Theta Z}r^2/R^2 + S_{ZZ})(m\pi/H)^2 - C_{\Theta\Theta\Theta\Theta}n^2 r^2/R^4, \\ \Lambda_{23} = \Lambda_{32} = -(C_{\Theta Z\Theta Z} + C_{\Theta\Theta ZZ})(nm\pi/H)\alpha r/R^2, \\ \Lambda_{33} = -C_{\Theta Z\Theta Z}n^2\alpha^2/R^2 - (C_{ZZZZ}\alpha^2 + S_{ZZ})(m\pi/H)^2. \end{cases} \quad (3.42)$$

Eqs. (3.17) and (3.41) must be solved simultaneously with respect to $\alpha$ and $r$ to obtain the bifurcation stretch and CNT radius for the given $(m,n)$ mode of the bifurcation displacement.

**Remark 3.** It is important to emphasize that all stresses and elasticities are averages (resultants) over a very thin wall of the CNT and their dimension is force per length (N/m) instead of the usual force per squared length (Pa). This is also in agreement with the fact that the representative volume element $V_0$ in Eq. (2.10) degenerates to the representative surface element $V_0 = 3\sqrt{3}L_0^2/4$ where $L_0$ is the interatomic distance in equilibrium.

### 3.3. Results

We present the results of numerical solution (for the critical CNT radius $r$ and stretch $\alpha$) of the coupled system of nonlinear bifurcation Eqs. (3.17) and (3.41) (see Fig. 5).
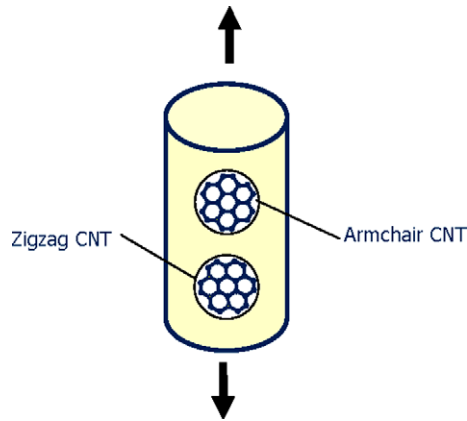
Fig. 5. Considered examples of the armchair and zigzag nanotubes.

First, we studied the convergence of the solution depending on the initial post-buckling mode presented by Eq. (3.40), i.e. as a function of the wave numbers $m$ and $n$. The critical strains and stress for nanotubes with an initial radius $R = 0.5$ nm and height $H = 5.0$ nm are presented in Fig. 6; they have remarkably different character for the zigzag and armchair CNTs. The zigzag CNT has the lowest critical point of bifurcation at $m = 1$ and $n = 0$, i.e. the symmetric bifurcation takes place. In the case of the armchair CNT $m = 1$ and $n > 4$ give the minimum critical parameters, i.e. asymmetric bifurcation takes place. We note that Zhang et al., who incorporate the three-body interaction, predict only symmetric bifurcations for both zigzag and armchair CNTs.
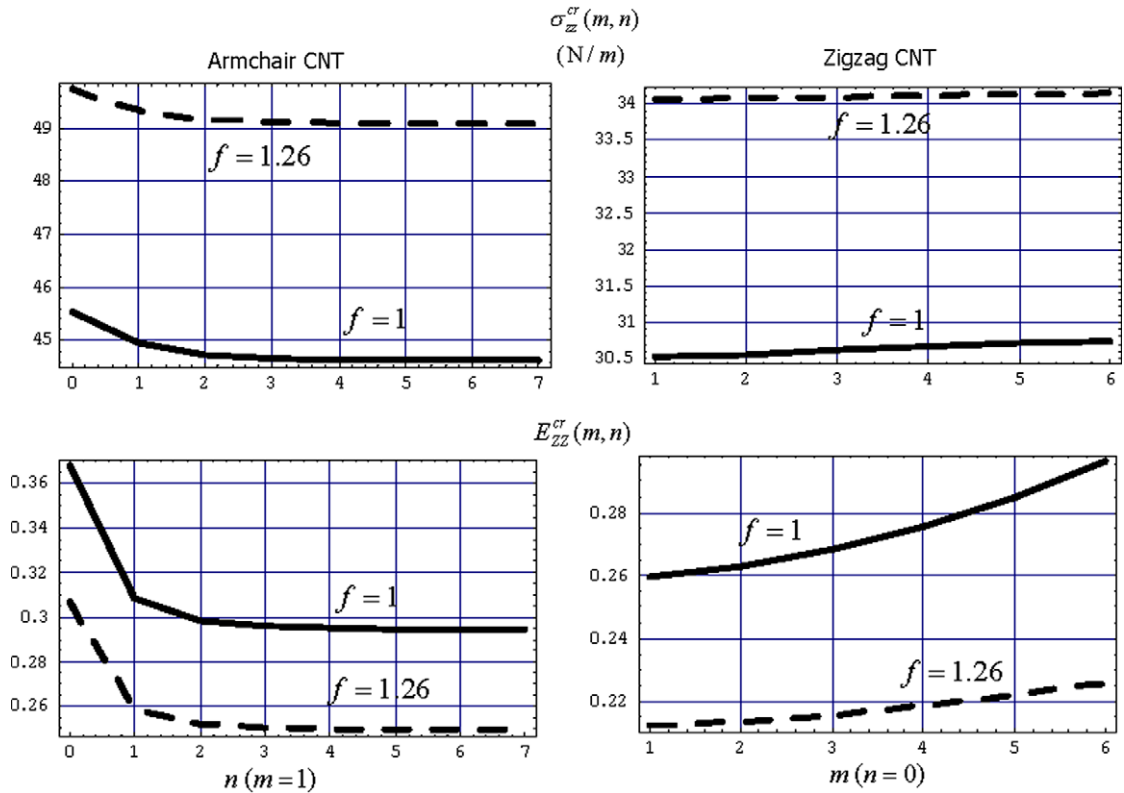


Fig. 6. Modal $(m,n)$ convergence of the critical (bifurcation) stress resultants and strains.

Second, we varied the 'multi-body stiffness' parameter $f$. Since the choice of parameter $f = 1.26$ connected with the multi-body atomic interactions was based on the experimental CNT Poisson ratio, which is approximate, it is desirable to explore the sensitivity of the solution of the bifurcation problem to the changing magnitude of this parameter. There is an increase of the CNT strength with the increase of $f$ (Fig. 7, top). However, the critical strains decrease with increasing $f$ (Fig. 7, bottom). This kind of 'embritllement' is characteristic of this particular continuum-atomistic model.

Third, we checked the sensitivity of the results with regard to the varying aspect ratio $R/H$ of the tubes. No sensitivity was found (Table 1).

Fourth, we compared the results of the bifurcation analysis based on the multi-body potential (2.32) with $f = 1.26$ and two-body potential with $f = 1$. As expected, the 'toughening' of the model is observed when the multi-body atomic interactions are included (Table 2).

Fifth, we tracked the stress–strain curves in the pre-bifurcation state – shown in Fig. 8. The initial slope (464 N/m for $f = 1.26$) of the curves is equivalent for both armchair (Fig. 8, top) and zigzag (Fig. 8, bottom) nanotubes. Since the crystalline structure of each nanotube is obtained from the other by $\pi/2$-rotation, it is possible to claim that the material is approximately isotropic for small strains. The latter justifies the idealization made in experimental measurements of the Poisson ratio.
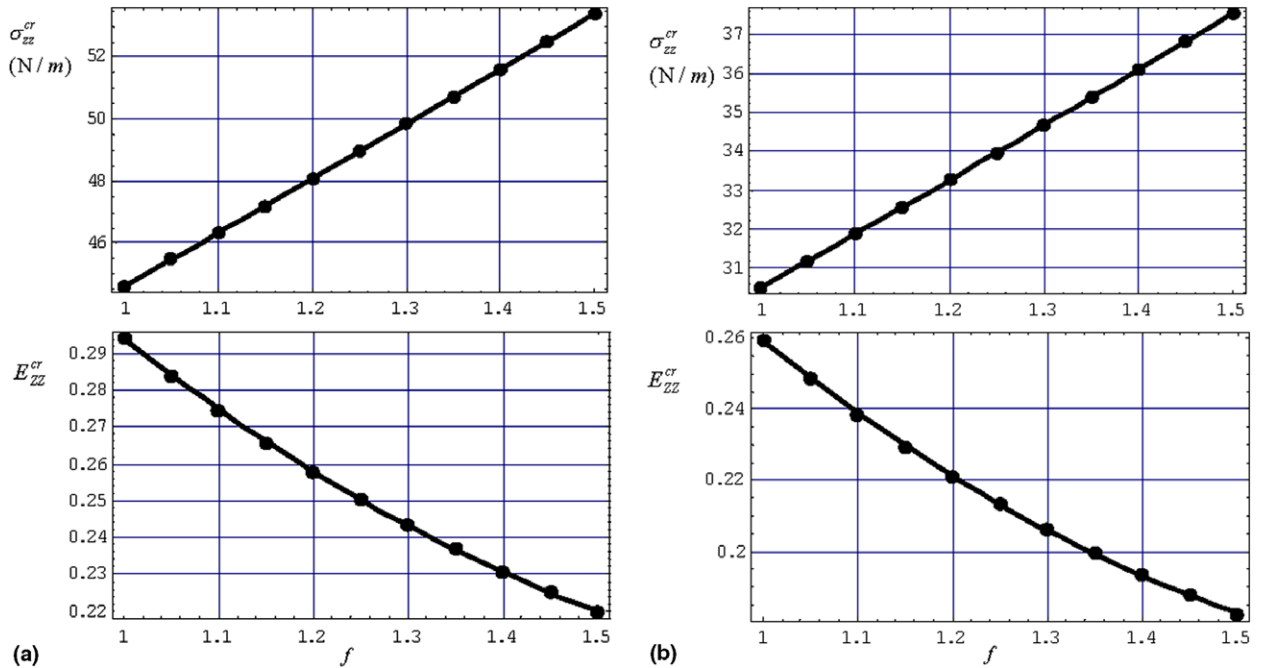


Fig. 7. Strength sensitivity of the armchair (a) and zigzag (b) CNTs to the varying multi-body stiffness ratio $f$.

Table 1
Critical strains and stress resultants ($f = 1.26$) for armchair (a) and zigzag (b) CNT as a function of varying aspect ratio

(a)

| $R/H$ | 0.05 | 0.10 | 0.15 | 0.20 | 0.25 |
|---|---|---|---|---|---|
| $E_{ZZ}^{cr}$ (%) | 25 | 25 | 25 | 25 | 25 |
| $\sigma_{zz}^{cr}$ (N/m) | 49 | 49 | 49 | 49 | 49 |

(b)

| $R/H$ | 0.05 | 0.10 | 0.15 | 0.20 | 0.25 |
|---|---|---|---|---|---|
| $E_{ZZ}^{cr}$ (%) | 21 | 21 | 21 | 21 | 21 |
| $\sigma_{zz}^{cr}$ (N/m) | 34 | 34 | 34 | 34 | 34 |

Table 2
Critical strains and stress resultants for two- and multi-body atomic interactions (Eq. (2.32))

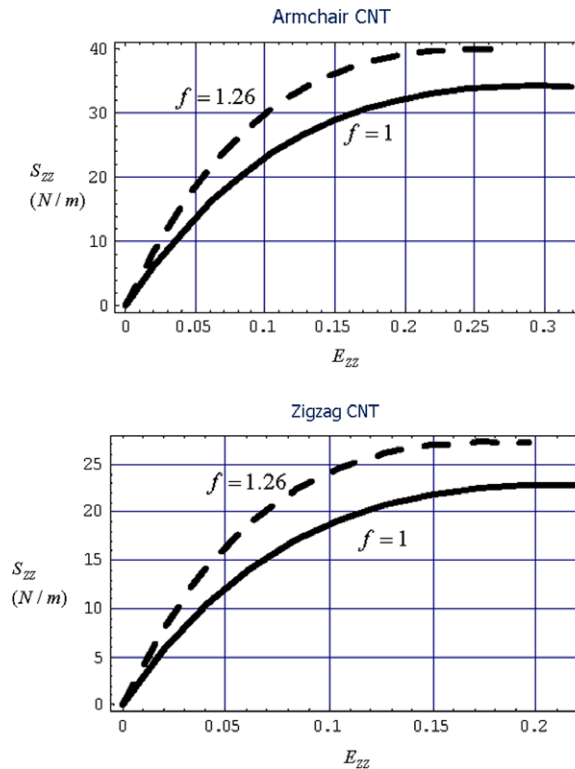|  | Two-body interactions $f = 1$ | Multi-body interaction $f = 1.26$ |  |
| --- | --- | --- | --- |
| $E_{ZZ}^{cr}$ (%) | 29 | 25 | Armchair |
|  | 26 | 21 | Zigzag |
| $\sigma_{zz}^{cr}$ (N/m) | 45 | 49 | Armchair |
|  | 31 | 34 | Zigzag |



Fig. 8. Second Piola–Kirchhoff stress (resultant) versus Green strain for pair- (solid line) and multi- (dashed lines) body potentials before bifurcation.

## 4. Discussion

The lack of experimental data on single-walled CNTs makes it difficult to asses the results of the theoretical analysis given in the present work directly. However, the work of Troiani et al. (2003) allows us to estimate the upper bound for the critical tensile strain. Using observations within a TEM, these authors reported that they observed 50% elongation of the single-walled nanotubes before *breaking*. Such an elongation corresponds to ∼62% Green strain. Our data for the *onset* of the tensile instability are 21–25% Green strain (for $f = 1.26$). Thus the necking occurs approximately between 20% and 60% Green strain, which seems reasonable. Some comparison with the experiments performed by Yu et al. (2000) on multi-walled CNTs is also possible. These authors measured the critical strain to be between 10% and 14% experimentally. Our results for critical strains are 21% for the zigzag CNT and 25% for the armchair CNT (for $f = 1.26$). Assuming that the addition of the wall layers leads to the stiffening of the CNT, the results of the theoretical analysis seem reasonable. Indeed, the critical strains are expected to decrease and the critical stresses are expected to increase with the CNT stiffening.

When comparing the results of theoretical predictions and experimental measurements, it should be recognized that idealized nano-structures are assumed in the analyses, while real imperfect nano-structures are tested in practice. It is extremely difficult to develop defect-free nanotubes, and this is a particular problem when the tensile instability will be modulated by the defects. The single SWCNT tests of Troiani et al. (2003) appear to be the closest to defect-free structures, and they appear to show the largest failure strains (note that these are failure strains, not the onset of the instability, which is what is predicted by this theoretical analysis). Other experiments (see, e.g. Yu (2004)) have generally shown a wide range of failure strains, typically significantly smaller, but these are typically in less-clean structures. The presence of atomic defects can disturb the results of the measurements. Further inclusion of the atomic imperfections in the theoretical models is of interest.

For the sake of comparison, our computations utilized the initial data of Zhang et al. (2004), who used the continuum-atomistic three-body Tersoff–Brenner potentials for simulating the multi-body interaction. The comparison of the results of Zhang et al. (2004) and of the present work can be summarized as follows:

- Zhang et al. (2004) predict 42% and 37% critical strains for the armchair and zigzag CNTs accordingly while the corresponding predictions of the present work are 25% and 21%, i.e. we predict lower critical strains.
- Zhang et al. (2004) predict symmetric bifurcation modes for both armchair and zigzag CNTs while the present work predicts symmetric bifurcation of the zigzag CNT and asymmetric bifurcation of the armchair CNT.
- Zhang et al. (2004) predict the aspect ratio sensitivity for zigzag CNTs contrary to the present work which predicts insensitivity of the tensile strength to the varying aspect ratio of the tube.

Commenting on this comparison summary we should note that our model gives lower critical strains because it is stiffer and 'more brittle' than the Tersoff–Brenner continuum-atomistic model developed by Zhang et al. (2004) and Jiang et al. (2003). The fact that our model is stiffer than that of Zhang et al. (2004) is evident in that the estimate of the Young's modulus by Zhang et al. (2002) is $E \approx 705$ GPa and our estimate $E \approx 1385$ GPa (this latter seems to be a better fit to numerous experimental and theoretical predictions reviewed in Fig. 1 of Zhang et al. (2004)). However, the assessment of the Young's modulus and stresses in the CNT is not trivial because the thickness of the CNT wall is difficult to define. The estimates of the Young's modulus given above were obtained with the assumption that the wall thickness is 0.335 nm (see Zhang et al., 2002). The fact that our model provides 'embrittlement' of the CNT mechanical response with the enforcement of the multi-body interactions is seen in Fig. 7 where a parametric study of the tensile strength of the armchair and zigzag CNTs is presented for the varying parameter of the multi-body interaction ($f$). The 'embrittlement' implies that the critical stress resultants increase while the critical strains decrease with the increasing magnitude of $f$. Comparing the bifurcation mode predictions we should mention that symmetric bifurcations are typical of the rod necking while asymmetric bifurcations are typical of the shell buckling. Our results predict that ideally perfect armchair nanotubes are shell-like while the zigzag nanotubes are rod-like in tension.

Concerning the detailed comparison of our results with those of Zhang et al. (2002, 2004) given above, we should clearly emphasize that our theory is not an approximation of the Tersoff–Brenner continuum-atomistic approach developed by Zhang et al. but a possible alternative to it. On the one hand, the physical strength of our proposal is in the fact that it allows accounting for the multi-body interactions without specifying the number of simultaneously interacting atoms. This is in contrast to the Tersoff–Brenner potential where the number of the interacting atoms is limited to three. On the other hand, the mathematical simplicity of our approach is in the fact that the pair structure of the continuum-atomistic potential is preserved. This is more efficient computationally.

## References

Abraham, F.F., Broughton, J.Q., Bernstein, N., Kaxiras, E., 1998. Spanning the continuum to quantum length scales in a dynamic simulation of brittle fracture. Europhys. Lett. 44, 783–787.

Alexandre, M., Dubois, P., 2000. Polymer-layered silicate nanocomposites: preparation, properties and uses of a new class of materials. Mater. Sci. Eng. R 28, 1–63.

Arroyo, M., Belytschko, T., 2002. An atomistic-based finite deformation membrane for single layer crystalline films. J. Mech. Phys. Solids 50, 1941–1977.

Beecrot, L.L., Ober, C.K., 1997. Nanocomposite materials for optical applications. Chem. Mater. 9, 1302–1317.

Belytschko, T., Xiao, S.P., Schatz, G.C., Ruo, R.S., 2002. Atomistic simulations of nanotube fracture. Phys. Rev. B 65, 235430-1–235430-8.

Born, M., Huang, K., 1954. Dynamical Theory of the Crystal Lattices. Oxford University Press, Oxford.

Brenner, D.W., 1990. Empirical potential for hydrocarbons for use in simulating the chemical vapor deposition of diamond films. Phys. Rev. B 42, 9458–9471.

Broughton, J.Q., Abraham, F.F., Bernstein, N., Kaxiras, E., 1999. Concurrent coupling of length scales: methodology and application. Phys. Rev. B 60, 2391–2403.

Gao, H., Klein, P., 1998. Numerical simulation of crack growth in an isotropic solid with randomized internal cohesive bonds. J. Mech. Phys. Solids 46, 187–218.

Goddard, W.A., Brenner, D.W., Lyshevski, S.E., Iafrate, G.J., 2003. Handbook of Nanoscience Engineering and Technology. CRC Press, London.

Dresselhaus, M.S., Dresselhaus, G., Eklund, P.C., 1996. Science of Fullerenes and Carbon Nanotubes. Academic Press, San Diego.

Ebbesen, T.W., Ajayan, P.M., 1992. Large-scale synthesis of carbon nanotubes. Nature 358, 220–222.

Harris, P.J.F., 1999. Carbon Nanotube and Related Structures: New Materials for the 21st Century. Cambridge University Press, Cambridge.

Krishnan, A., Dujardin, E., Ebbesen, T.W., Yianilos, P.N., Treacy, M.M.J., 1998. Young's modulus of single-walled nanotubes. Phys. Rev. B 58, 14013–14019.

Iijima, S., 1991. microtubules of graphite carbon. Nature 354, 56–58.

Jiang, H., Zhang, P., Liu, B., Huang, Y., Geubelle, P.H., Gao, H., Hwang, K.C., 2003. The effect of nanotube radius on the constitutive model for carbon nanotubes. Comput. Mater. Sci. 28, 429–442.

Klein, P., Gao, H., 1998. Crack nucleation and growth as strain localization in a virtual-bond continuum. Eng. Fract. Mech. 61, 21–48.

Klein, P., Gao, H., 2000. Study of crack dynamics using the virtual internal bond method. In: Multiscale Deformation and Fracture in Materials and Structures. Kluwer Academic Publishers, Dodrecht, pp. 275–309.

Liu, W.K., Karpov, E.G., Zhang, S., Park, H.S., 2004. An introduction to computational nanomechanics and materials. Comput. Meth. Appl. Mech. Eng. 193, 1529–1578.

Lourie, O., Wagner, H.D., 1998a. Evaluation of Young's modulus of carbon nanotubes by micro-Raman spectroscopy. J. Mater. Res. 13, 2418–2422.

Lourie, O., Wagner, H.D., 1998b. Transmission electron microscopy observations of fracture of single-wall carbon nanotubes under axial tension. Appl. Phys. Lett. 73, 3527–3529.

Marques, M.A.L., Troiani, H.E., Miki-Yoshida, M., Jose-Yacaman, M., Rubio, A., 2004. On the breaking of carbon nanotubes under tension. Nanoletters 4 (5), 811–815.

Meyyappan, M. (Ed.), 2005. Carbon Nanotubes: Science and Applications. CRC Press, Boca Raton.

Miller, R., Tadmor, E.B., Phillips, R., Ortiz, M., 1998. Quasicontinuum simulation of fracture at the atomic scale. Model. Simul. Mater. Sci. Eng. 6, 607–638.

Muster, J., Burghard, M., Roth, S., Duesberg, G.S., Hernandez, E., Rubio, A., 1998. Scanning force microscopy characterization of individual carbon nanotubes on electrode arrays. J. Vac. Sci. Technol. B 16, 2796–2801.

Odegard, G.M., Gates, T.S., Nicholson, L.M., Wise, K.E., 2002. Equivalent-continuum modeling of nano-structured materials. Compos. Sci. Technol. 62, 1869–1880.

Ortiz, M., Cuitino, A.M., Knap, J., Koslowski, M., 2001. Mixed atomistic continuum models of material behavior: the art of transcending atomistics and informing continua. MRS Bull. 26, 216–221.

Pan, Z.W., Xie, S.S., Lu, L., Chang, B.H., Sun, L.F., Zhou, W.Y., Wang, G., 1999. Tensile tests of ropes of very long aligned multi-wall carbon nanotubes. Appl. Phys. Lett. 74, 3152–3154.

Qian, D., Wagner, G.J., Liu, W.K., Yu, M.F., Ruo, R.S., 2002. Mechanics of carbon nanotubes. Appl. Mech. Rev. 55, 495–533.

Reich, S., Thomsen, C., Maultzsch, J., 2004. Carbon Nanotubes. Wiley-VCH, Weinheim, Germany.

Salvetat, J.-P., Briggs, G.A.D., Bonard, J.-M., Bacsa, R.R., Kulik, A.J., 1999. Elastic and shear moduli of single-walled carbon nanotube ropes. Phys. Rev. Lett. 82, 944–947.

Shenoy, V.B., Miller, R., Tadmor, E.B., Phillips, R., Ortiz, M., 1998. Quasicontinuum models of interfacial structure and deformation. Phys. Rev. Lett. 80, 742–745.

Tadmor, E.B., Ortiz, M., Phillips, R., 1996. Quasicontinuum analysis of defects in solids. Philos. Mag. A 73, 1529–1563.

Tadmor, E.B., Smith, G.S., Bernstein, N., Kaxiras, E., 1999. Mixed finite element and atomistic formulation for complex crystals. Phys. Rev. B 59, 235–245.

Tersoff, J., 1988. New empirical approach for the structure and energy of covalent systems. Phys. Rev. B 37, 6991–7000.

Thess, A., Lee, R., Nikolaev, P., Dai, H.J., Petit, P., Robert, J., Xu, C.H., Lee, Y.H., Kim, S.G., Rinzler, A.G., Colbert, D.T., Scuseria, G.E., Tomanek, D., Fischer, J.E., Smalley, R.E., 1996. Crystalline ropes of metallic carbon nanotubes. Science 273, 483–487.

Tombler, T.W., Zhou, C., Alexseyev, L., Kong, J., Dai, H., Liu, L., Jayanthi, C.S., Tang, M., Wu, S.-Y., 2000. Reversible electromechanical characteristics of carbon nanotubes under local-probe manipulation. Nature 405, 769–772.

Treacy, M.M.J., Ebbesen, T.W., Gibson, J.M., 1996. Exceptionally high Young's modulus observed for individual carbon nanotubes. Nature 381, 678–680.

Troiani, H.E., Miki-Yoshida, M., Camacho-Bragado, G.A., Marques, M.A.L., Rubio, A., Ascencio, J.A., Jose-Yacaman, M., 2003. Direct observation of the mechanical properties of single-walled carbon nanotubes and their junctions at the atomic level. Nanoletters 3 (6), 751–755.

Volokh, K.Y., 2004. Nonlinear elasticity for modeling fracture of isotropic brittle solids. J. Appl. Mech. ASME 71, 141–143.

Volokh, K.Y., Gao, H., 2005. On the modified virtual internal bond method. J. Appl. Mech. ASME 72, 969–971.

Weiner, J.H., 1983. Statistical Mechanics of Elasticity. Wiley, New York.

Wong, E.W., Sheehan, P.E., Lieber, C.M., 1997. Nanobeam mechanics: elasticity, strength, and toughness of nanorods and nanotubes. Science 277, 1971–1975.

Yakobson, B.I., Campbell, M.P., Brabec, C.J., Bernholc, J., 1997. High strain rate fracture and C-chain unraveling in carbon nanotubes. Comput. Mater. Sci. 8, 341–348.

Yu, M.-F., Lourie, O., Dyer, M.J., Moloni, K., Kelly, T.F., Ruo, R.S., 2000. Strength and breaking mechanism of multi-walled carbon nanotubes under tensile load. Science 287, 637–640.

Yu, M.-F., 2004. Fundamental mechanical properties of carbon nanotubes: current understanding and the related experimental studies. J. Eng. Mater. Technol. 126, 271–278.

Zhang, P., Huang, Y., Geubelle, P.H., Klein, P.A., Hwang, K.C., 2002. The elastic modulus of single-wall carbon nanotubes: a continuum analysis incorporating interatomic potentials. Int. J. Solids Struct. 39, 3893–3906.

Zhang, P., Jiang, H., Huang, Y., Geubelle, P.H., Hwang, K.C., 2004. An atomistic-based continuum theory for carbon nanotubes: analysis of fracture nucleation. J. Mech. Phys. Solids 52, 977–998.